Korean J. of Chem. Eng., **13**(2), 136-143 (1996)

LOW DIMENSIONAL MODELING OF TURBULENT THERMAL CONVECTION

Hung Mok Park

Department of Chemical Engineering, Sogang University, Seoul, Korea
(Received 20 April 1995 • accepted 12 January 1996)

Abstract—The Karhunen-Loeve decomposition is used to obtain a low dimensional model describing the dynamics of turbulent thermal convection in a finite box. The Karhunen-Loeve decomposition is a procedure for decomposing a stochastic field in an optimal way such that the stochastic field can be represented with a minimum number of degree of freedom. Numerical data for the turbulent thermal convection, generated by a pseudo-spectral method for the case of Pr=0.72 and aspect ratio=2, are processed by means of Karhunen-Loeve decomposition to yield a set of empirical eigenfunctions. A Galerkin procedure employing this set of empirical eigenfunctions reduces the Boussinesq equation to a small number of ordinary differential equations. This low dimensional model obtained from numerical data at the reference Rayleigh number of 70 times the critical Rayleigh number is found to predict turbulent convection reasonably well over a range of Rayleigh numbers around the reference value.

Key words: Turbulence, Thermal Convection, Karhunen-Loeve Decomposition, Direct Spectral Simulation, Low Dimensional Dynamics

INTRODUCTION

Although the Rayleigh-Benard convection in turbulent state has been subject to a long history of experimental work [Silvestone, 1958], its numerical simulation is rather new. It is only recent years when large scale computer simulations have been performed for Rayleigh-Benard convection well into the chaotic or turbulent regime [Grötzbach, 1983; Herring and Wyngaard, 1986; Kessler, 1987; McLaughlin and Orszag, 1982]. In some sense one might consider numerical simulations as a new experimental tool, but one in which one has much more control over the experimental conditions than in the laboratory experiment, and one in which more detailed results may be obtained than in the laboratory. Also, in numerical simulation one can obtain information about quantities that are difficult or impossible to measure in the laboratory. In this approach, we resolve numerically all small scale motions of turbulence, which is inherently three-dimensional and unsteady, without introducing any turbulence models such as k-epsilon models, etc. This approach, called direct numerical simulation, demands tremendous amount of computer time and computer memory since we need a very large number of grids to resolve all small scale motions, and as a result produces a vast amount of numerical data or informations. We encounter the same situation in laboratory experiments if all details of turbulence are measured. Therefore, the analysis and the assessment of huge data sets are nowadays one of the central problems confronting turbulence research. The number of scales of motion activated in turbulence has a close relationship with the degree of freedom or the dimension of the underlying turbulence dynamics. For a clear understanding as well as practical applicability of the dynamic models of turbulence, it is essential for these dynamic models to be low dimensional.

In many physical systems described by nonlinear partial differential equations including the turbulent Rayleigh-Benard convection under consideration in the present paper, the representational space is very large or infinite. As an example, we recall Landau's estimate on the degrees of freedom present in a given flow. Using the Kolmogorov scale as an estimate of the smallest relevant scale he arrived at $(Re/Re_c)^{9/4}$ degree of freedom, where Re_c is the critical Reynolds number. By making use of Stoke's eigenfunctions, Constantine et al. [1985] obtained a similar estimate with the use of a rigorous mathematical analysis. But based on many previous numerical and experimental evidence [Brown and Roshko, 1974] we conjecture that a description involving a much smaller space is possible. One clear and systematic way of demonstrating this conjecture is to employ the Karhunen-Loeve decomposition (K-L decomposition), a brief description of which is given in Sec. 2.

The Karhunen-Loeve decomposition is first suggested by Lumley [1967] and Sirovich [1987a, 1987b] as a rational procedure for the extraction of characteristic structures of turbulent flow fields. Those characteristic structures are called empirical eigenfunctions. As originally presented by Lumley, the method becomes impractical unless all but one of the directions have periodic boundary conditions. Due to this limitation, most of applications of the Karhunen-Loeve decomposition to turbulence have been confined to systems with periodic conditions. Perhaps one distinguished exception is the turbulent Rayleigh-Benard in a confined domain considered by Park and Sirovich [1990] and Sirovich and Park [1990] where no periodicity of boundary conditions is imposed. For a confined domain, the empirical eigenfunctions appear as complicated functions not expressible analytically, which are in contrast with those of infinite domains with periodic boundaries whose empirical eigenfunctions are sinusoidal in the periodic directions. In this fully confined turbulent R-B convection problem, the difficulty in the original form of the Karhunen-Loeve decomposition has been overcome by using the method of snapshot or Schmidt-Hilbert technique. In this way, the applicability of the K-L decomposition has been extended to a more practical situation.

When the K-L decomposition is applied to the turbulent Rayleigh-Benard convection in a c nfined domain, as explained in

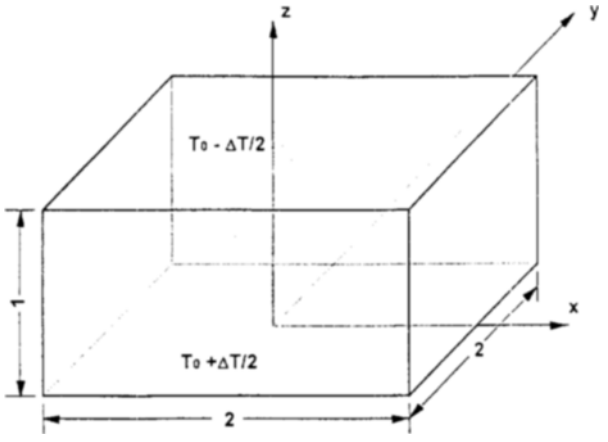

Fig. 1. Flow geometry.

our previous work [Park and Sirovich, 1990; Sirovich and Park, 1990], the low dimensionality of the underlying dynamics of turbulence is clearly exhibited by the rapid convergence of the K-L procedure, i.e., most of the turbulence energy is captured with only a small number of empirical eigenfunctions. The empirical eigenfunctions generated in the Karhunen-Loeve procedure can be used very efficiently in a Galerkin procedure to generate a low dimensional dynamic system [Aubry et al., 1988; Sirovich, 1987b].

In the present work we use the empirical eigenfunctions of the Rayleigh-Benard convection in a finite domain to approximate the dynamic behavior of the corresponding system. As is demonstrated in the previous work on the Ginzburg-Landau equation [Sirovich and Rodriguez, 1987], the eigenfunctions generated for a fixed control parameter can be used to describe the dynamics of the system at other parameter values as long as these values are not much larger than the original one. Usually in turbulent flow, as the Reynolds number (Rayleigh number R in the case of thermal convection) increases, more and more small scale motions (eddies) appear. But the large scale motions, for example coherent structures, take care of most of the turbulent energy and have a dominant role in determining the transfer rates of momentum, heat and mass, that may be one of the most important aspects of turbulence in engineering applications. As will be demonstrated in the sequel, the Karhunen-Loeve decomposition yields empirical eigenfunctions in the order of the size of the scales of flow and suggests a very convenient tool of obtaining a low dimensional model for turbulent dynamics. It shall be demonstrated that this low dimensional model can be used to predict phenomena of large scale motions of turbulence, such as Nusselt number, over a range of Rayleigh numbers.

GOVERNING EQUATIONS AND THE KARHUNEN-LOEVE DECOMPOSITION

The physical system of our specific interest in the present work is the Rayleigh-Benard convection in a finite domain as sketched in Fig. 1. The Boussinesq equation and boundary conditions for this investigation are to be found in Sirovich and Park [1990] and are repeated here in the following form.

$$\nabla \cdot \mathbf{u} = 0 \tag{1}$$

$$\frac{\partial \mathbf{u}}{\partial t} - \mathbf{u} \wedge \omega = -\nabla\left(p + \frac{u^2}{2}\right) + R\ Pr\ T\ \mathbf{e}_z + Pr\ \nabla^2 \mathbf{u} \tag{2}$$

$$\frac{\partial T}{\partial t} + \mathbf{u} \cdot \nabla T = w + \nabla^2 T \tag{3}$$

where ω is vorticity and (u, v, w) the components of the velocity vector $\mathbf{u}$, R the Rayleigh number, Pr the Prandtl number, and T is the deviation temperature given by the difference between the system temperature T_{total} and the basic conduction profile, $T_0 + (T_1 - T_0)z/H$, thus $T_{total} \equiv T + T_0 + (T_1 - T_0)z/H$. Here, T_0 is the bottom temperature, T_1 is the top temperature and H is the system height. The relevant boundary conditions are as follows.

$$w = T = \frac{\partial u}{\partial z} = \frac{\partial v}{\partial z} = 0 \qquad \text{at } z = 0,\ 1 \tag{4}$$

$$u = \frac{\partial T}{\partial x} = \frac{\partial v}{\partial x} = \frac{\partial w}{\partial x} = 0 \qquad \text{at } x = 0,\ 2 \tag{5}$$

$$v = \frac{\partial T}{\partial y} = \frac{\partial u}{\partial y} = \frac{\partial w}{\partial y} = 0 \qquad \text{at } y = 0,\ 2 \tag{6}$$

These boundary conditions specify slip momentum boundary conditions at all boundaries, adiabatic sidewalls and specified temperatures at the upper and lower boundaries. These boundary conditions may correspond to situations similar to free shear layers, which is more difficult to be realized experimentally than the usual non-slip boundaries. But this shear-free boundary conditions greatly reduce the computation cost because we can employ Fourier expansion instead of Chebyshev expansion in the spectral simulation. The aspect ratio of 2 includes the most dangerous mode from linear stability theory [Sirovich and Park, 1990]. The Rayleigh number is 70 times the critical value and Pr equals 0.72. The critical Rayleigh number for this case is 657.5. The Pr value adopted here is that of air which is one of the most common fluids available. In Rayleigh-Benard convection, the Prandtl number has non-negligible effect on instability or transition, where the Rayleigh number is around the critical value. But when the Rayleigh number exceeds far more than the critical value, as is in the present work, the effect of Prandtl number on the Rayleigh-Benard convection, especially on Nusselt number, is negligible. This is well demonstrated by the classical experiment of Silveston [1958], who used various fluids having widely different values of Pr and measured Nusselt number as a function of Rayleigh number. His result, that is also cited as Fig. 13 in Chandrasekhar [1961], reveals that the Nusselt number does not depend appreciably on Prandtl number in turbulent thermal convection. But it may be interesting to investigate the effect of Pr on turbulent thermal convection in detail in the future.

The numerical procedure is as follows. We generate snapshots of the flow field by solving Eqs. (1)-(6) with a pseudospectral method. Algebraic products are calculated in the physical space and derivatives in the Fourier space, and the fast Fourier transform allows rapid passage between the spaces. This follows standard practice [Canuto et al., 1988]. A time marching scheme based on a leap-frog for nonlinear terms and an exact integration for the linear part is employed, which is stabilized by a periodic use of a second order Runge-Kutta scheme. The time step of integration is taken to be less than the Kolmogorov time scale ($\Delta t = 0.001$) and the number of grid points is large enough to resolve the Kolmogorov microscale (17^3 grids). The velocity and temperature fields are dumped at every 600 time steps to generate 200

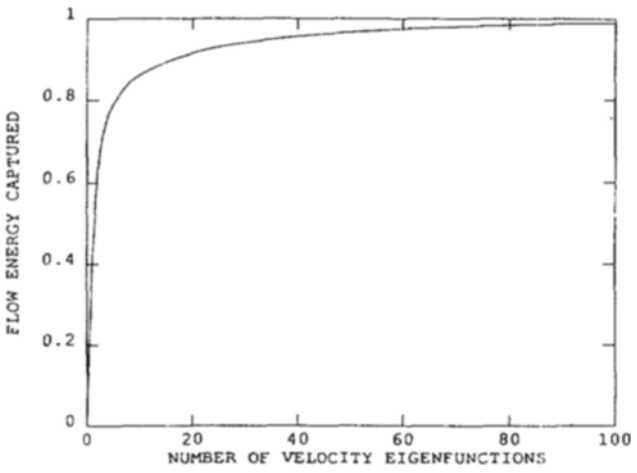

Fig. 2a. The variation of velocity energy captured versus the number of velocity empirical eigenfunctions.

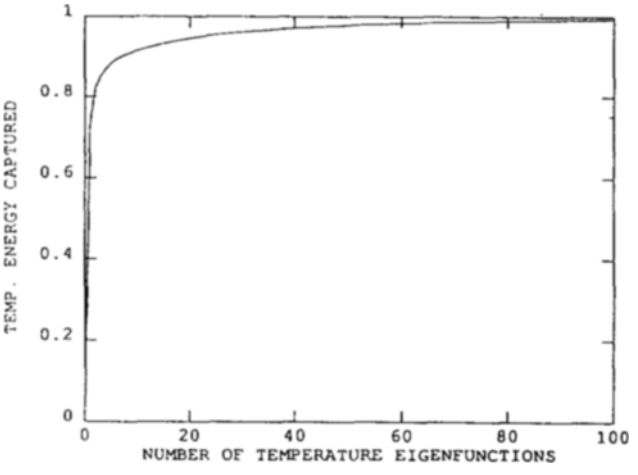

Fig. 2b. The variations of temperature energy captured versus the number of temperature empirical eigenfunctions.

snapshots which are used as a data set for the subsequent Karhunen-Loeve decomposition. In Park and Sirovich [1990] we reported the detail of numerical method and the empirical eigenfunctions obtained by the snapshot method. Here a slightly different set of eigenfunctions is obtained, which is more convenient as a set of basis functions for the Galerkin approximation. The difference is that now we separate the velocity and temperature fields when constructing the kernel of the Karhunen-Loeve integral equation.

We take the state variables to be

$$\mathbf{u}=(v_1,\ v_2,\ v_3) \tag{7}$$

where v_1, v_2 and v_3 are the velocity components in the Cartesian coordinates, and imagine an ensemble of states (snapshots) of the flow on the attractor, denoted by

$$\mathbf{u}^{(n)}=\mathbf{u}(\mathbf{x},\ t_n) \tag{8}$$

and sampled at uncorrelated times t_n. The eigenfunction of the following integral equation with the largest eigenvalue λ has the interpretation of being the most likely state of the flow field.

$$\int \mathbf{K}(\mathbf{x},\ \mathbf{x}')\ \boldsymbol{\Phi}(\mathbf{x}')d\mathbf{x}'=\lambda\boldsymbol{\Phi}(\mathbf{x}) \tag{9}$$

where

$$[\mathbf{K}]_{ij}=K_{ij}(\mathbf{x},\ \mathbf{x}')=\langle v_i(\mathbf{x})v_j(\mathbf{x}')\rangle\equiv\frac{1}{N}\sum_{n=1}^{N} v_j^{(n)}(\mathbf{x})v_j^{(n)}(\mathbf{x}') \tag{10}$$

is the two point correlation function. The eigenfunction $\boldsymbol{\Phi}$ with the next largest eigenvalue is the next likely state and so forth. This set of empirical eigenfunctions $\{\boldsymbol{\Phi}_j\}$ satisfy orthogonality,

$$(\boldsymbol{\Phi}_j,\ \boldsymbol{\Phi}_k)=\int_\Omega \boldsymbol{\Phi}_j\cdot\boldsymbol{\Phi}_k\ d\mathbf{x}=0,\ j\neq k \tag{11}$$

and are solenoidal, $\nabla\cdot\boldsymbol{\Phi}_j=0$. Similarly the integral equation yielding empirical eigenfunctions for the temperature field is given by

$$\int K(\mathbf{x},\ \mathbf{x}')\psi(\mathbf{x}')d\mathbf{x}'=\lambda\psi(\mathbf{x}) \tag{12}$$

where

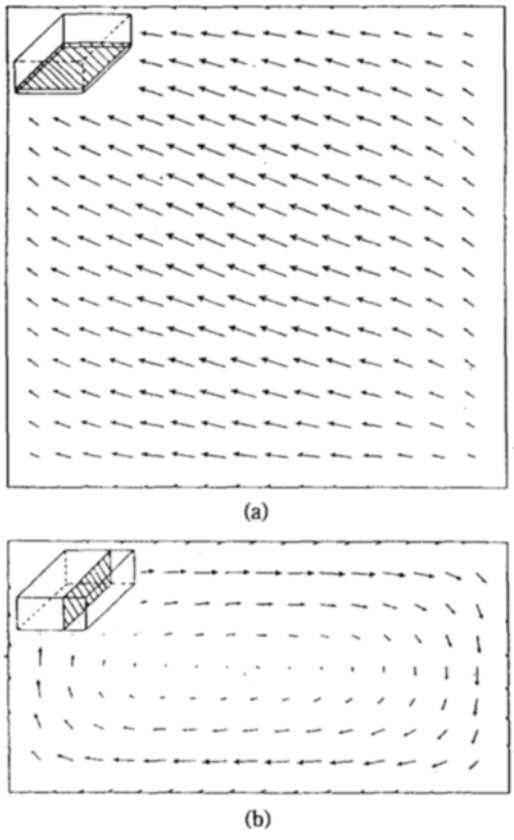

Fig. 3a, b. The cross sectional views of the dominant velocity eigenfunction. Inserts indicate planes in which flow lines are shown.

$$K(\mathbf{x},\ \mathbf{x}')=\langle T(\mathbf{x})T(\mathbf{x}')\rangle\equiv\frac{1}{N}\sum_{n=1}^{N} T^{(n)}(\mathbf{x})T^{(n)}(\mathbf{x}') \tag{13}$$

and the set $\{\psi_j\}$ is orthogonal. Figs. 2a and 2b plot the variation of energy capture versus the number of velocity and temperature eigenfunctions. Thus, with 50 eigenfunctions 95% of flow energy and 97% of temperature energy are captured. Figs. 3 and 4 show the dominant velocity and temperature eigenfunctions (i.e., eigen-

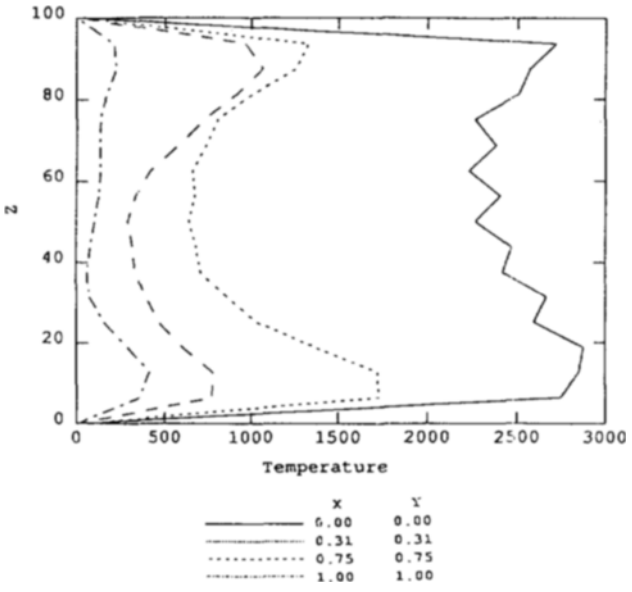

Fig. 4. The second temperature eigenfunction. Plotted are the vertical variation of temperature at several (x, y) locations; the center of the horizontal plane (x, y) is (1.0, 1.0) and the corner (0.0, 0.0).

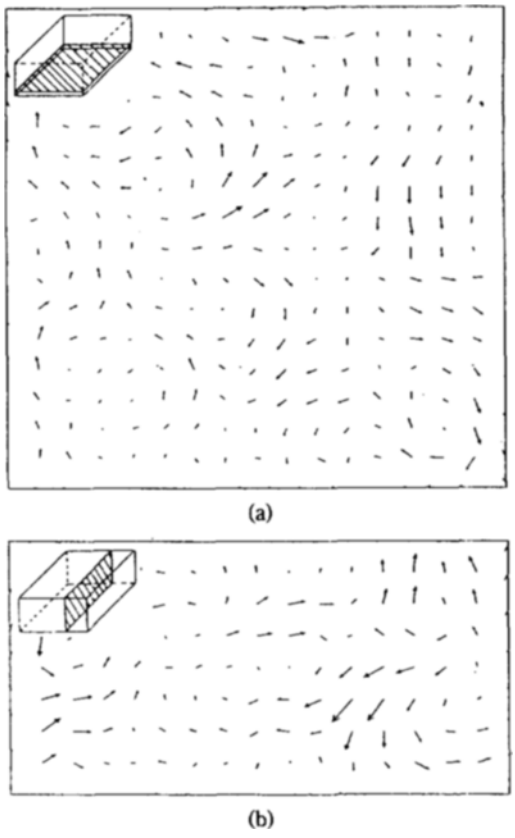

Fig. 5a, b. The 50th velocity eigenfunction; inserts indicate planes in which flow lines are shown.

functions with large eigenvalues). They depict large scale, energetic motions of turbulent flow field. These dominant eigenfunctions are characterized by relatively well-organized large scale

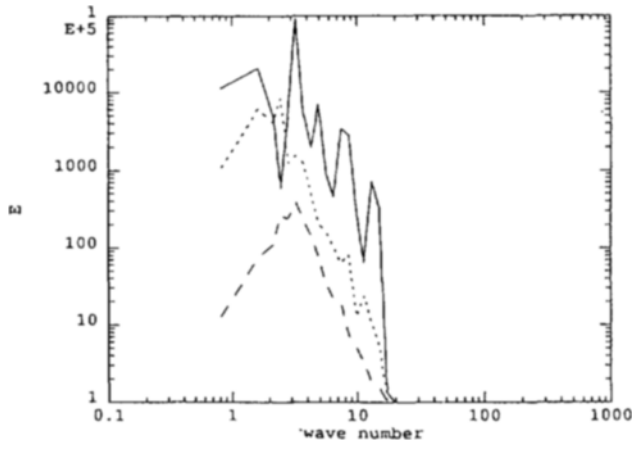

Fig. 6. Energy spectrum of the first (solid line —), the 10th (dotted line ···), and the 50th (dashed line ---) velocity empirical eigenfunctions.

motions. By contrast eigenfunctions of high index as typified in Fig. 5, reveal irregular chaotic motion of much smaller length scale. This shows that through the K-L decomposition, large scale motions are depicted by dominant eigenfunctions and small scale motions which correspond to high frequency part of flow field are captured by eigenfunctions with smaller eigenvalues. Fig. 6 shows the energy spectra of the first, the 10th and the 50th velocity eigenfunction respectively. These energy spectra show that the empirical eigenfunctions are not monochromatic in spectral space but have broad band structures with maxima appearing at certain frequencies which represent the dominant scales for the corresponding eigenfunctions. The dominant eigenfunctions, such as the first one, have peaks at spatial frequencies which characterize their specific shapes. As the eigenvalue decreases the spatial frequency which yields maximum energy spectrum increases and the spectrum becomes more broad banded (in the sense that the standard deviation becomes larger). This is an indication of the existence of many small scale motions of different sizes.

The above trend suggests that the eigenfunctions with small eigenvalues act as eddy viscosity in the dynamics of large scale motion depicted by eigenfunctions with large eigenvalues. When we employ these empirical eigenfunctions as basis functions for the Galerkin procedure, as described in the next section, only a finite number of them are used and the remaining empirical eigenfunctions of high index (with smaller eigenvalues) are truncated. The resulting low dimensional dynamic system from this Galerkin procedure may be deficient in effective viscosity, especially when the control parameters, like the Rayleigh number, exceed the value at which the empirical eigenfunctions have been obtained. This fact will be explained further in the subsequent sections.

THE GALERKIN PROCEDURE

Next we project the Boussinesq equation into a finite dimensional space by means of a Galerkin procedure. Exploiting the fact that the Karhunen-Loeve decomposition produces a set of eigenfunctions in the order of their importance in describing the chaotic turbulent flow field, we first write,

$$\mathbf{u}=\begin{bmatrix}u\\v\\w\end{bmatrix}=\sum_{n=1}^{MM} a_n(t)\phi_n(\mathbf{x}) \tag{14}$$

$$T=\sum_{n=1}^{MT} b_n(t)\psi_n(\mathbf{x}) \tag{15}$$

where MM is the number of velocity eigenfunctions and MT that of temperature eigenfunctions employed in the Galerkin procedure. It may be convenient to take MM and MT to be the same number, but it does not always have to be so. As before $\{\phi_n\}$ is the set of velocity eigenfunctions and $\{\psi_n\}$ the set of temperature eigenfunctions presented in the order of magnitude of eigenvalues. These expansions (14) and (15) satisfy the boundary conditions (4)-(6) automatically since each of the empirical eigenfunctions ϕ_n and ψ_n satisfies all the boundary conditions (4)-(6).

On substituting these Eqs. (14) and (15) into the set of Boussinesq Eqs. (1)-(3) and requiring the residuals be orthogonal to each of the basis functions used in the expansion, we find the following coupled set of ordinary differential equations in eigenfunction space.

$$S_k\frac{da^{(k)}}{dt}=\sum_{l=1}^{MM}\sum_{m=1}^{MM} a^{(l)}a^{(m)}Q_{klm}+Pr\sum_{l=1}^{MM} a^{(l)}A_{kl}+RPr\sum_{l=1}^{MT} b^{(l)}C_{kl},\quad k=1,\cdots,MM \tag{16}$$

$$P_k\frac{db^{(k)}}{dt}=-\sum_{l=1}^{MM}\sum_{m=1}^{MT} a^{(l)}b^{(m)}R_{klm}+\sum_{l=1}^{MT} b^{(l)}B_{kl}+\sum_{l=1}^{MM} a^{(l)}D_{kl},\quad k=1,\cdots,MT \tag{17}$$

where

$$S_k\equiv\int_\Omega \phi_k\cdot\phi_k d\mathbf{x} \tag{18}$$

$$P_k\equiv\int_\Omega \psi_k\psi_k d\mathbf{x} \tag{19}$$

$$Q_{klm}\equiv\int_\Omega \phi_k\cdot\{\phi_l\wedge(\nabla\wedge\phi_m)\}d\mathbf{x} \tag{20}$$

$$R_{klm}\equiv\int_\Omega \psi_k\{\nabla\cdot(\phi_l\psi_m)\}d\mathbf{x} \tag{21}$$

$$A_{kl}\equiv\int_\Omega \phi_k\cdot\nabla^2\phi_l d\mathbf{x} \tag{22}$$

$$B_{kl}\equiv\int_\Omega \psi_k\nabla^2\psi_l d\mathbf{x} \tag{23}$$

$$C_{kl}\equiv\int_\Omega \phi_k^w\psi_l d\mathbf{x} \tag{24}$$

$$D_{kl}\equiv\int_\Omega \psi_k\phi_l^w d\mathbf{x} \tag{25}$$

In the above equations, ϕ_k^w is the z-component of the velocity eigenfunction ϕ_k.

The resulting sets of ordinary differential Eqs. (16) and (17) constitute the low dimensional model for turbulent thermal convection in the finite domain considered in the present work. This low dimensional model may be thought to be based on the following picture of turbulence. Namely, we imagine a chaotic and complicated turbulent flow field is composed of empirical eigenfunctions.

$$\mathbf{u}(\mathbf{x},\ t)=\sum_{n=1}^{\infty} a_n(t)\phi_n(\mathbf{x}) \tag{26}$$

where the time dependent coefficients $a_n(t)$'s are given by

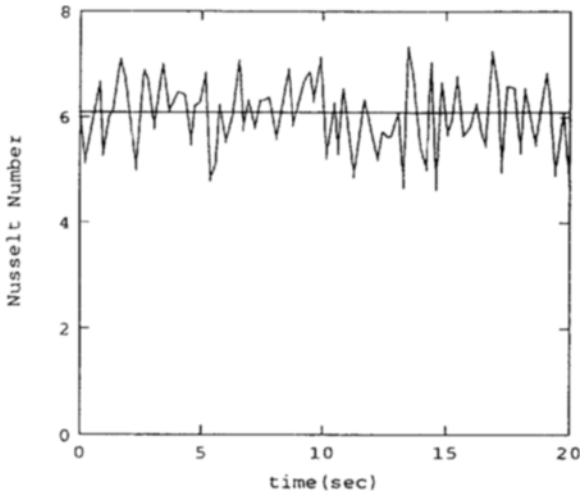

Fig. 7. Time series of the area averaged Nusselt number for $R=70R_C$ from the low dimensional dynamic system.

$$a_n(t)=\int_\Omega \mathbf{u}\cdot\phi_n d\mathbf{x} \tag{27}$$

The interpretation of Eqs. (26) and (27) is that the "unsteady" complicated turbulent flow field is modeled to be composed of sum of "steady" deterministic empirical eigenfunctions, and the unsteadiness of turbulence comes from the time dependence of the coefficients a_n's that premultiply each eigenfunction. The resulting low dimensional Eqs. (16) and (17) are solved by a fourth-order Runge-Kutta method.

RESULTS AND DISCUSSION

In this section we shall investigate how well the low dimensional system of the present work reproduces the results of the original dynamics, i.e., the Boussinesq set of Eqs. (1)-(3). For this purpose we set, as a reference value, MM=100 and MT=100, where MM is the number of velocity eigenfunctions and MT that of temperature eigenfunctions respectively. This set of 200 ordinary differential equations is integrated for 20 physical seconds to generate a time series of area-averaged Nusselt number and averaged profiles for $\langle T\rangle_A$ where $\langle\cdot\rangle_A$ means horizontal area average. Since the system temperature is given as $T_{total}=T+T_0+(T_1-T_0)z/H$, the Nusselt number is defined by $Nu=1-(\partial T/\partial Z)/(T_0-T_1/H)$. The integration time of 20 physical seconds is sufficiently long to get stationary turbulence statistics. In the following, the Prandtl number is fixed to be 0.72 for all results. Fig. 7 shows the time series of the unsteady area-averaged Nusselt number, i.e. $\langle Nu\rangle_A$, for R=70Rc when the reference Rayleigh number, on which the original empirical eigenfunctions are based, is the same $70R_C$. Here R_C is the critical Rayleigh number based on a linear stability analysis [Sirovich and Park, 1990]. The time averaged Nusselt number from this low dimensional model is 6.05 which is 5% higher than the exact value of 5.75 [Park and Sirovich, 1990]. Considering the fact that 98% of the velocity energy and 99% of the temperature energy are captured with 100 empirical eigenfunctions (cf. Fig. 2a, b) and the Nusselt number is determined by a temperature gradient which is not so easily captured as the temperature itself through the empirical eigenfunctions, this accuracy of prediction is more than what we can expect. The horizontal area averaged temperature profile $\langle T\rangle_A$

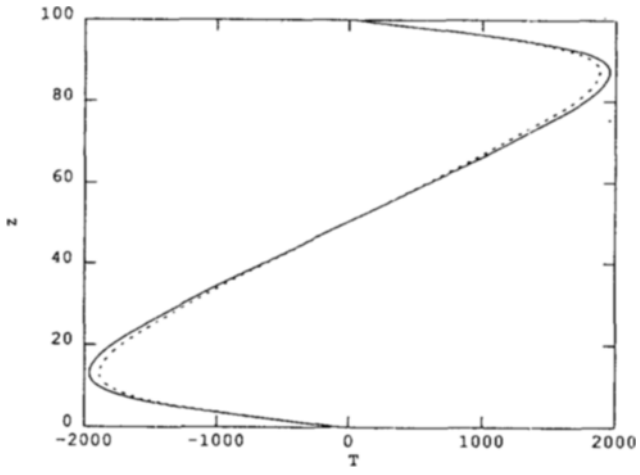

Fig. 8. Horizontal area averaged temperature profile $\langle T \rangle_A$ obtained from the low dimensional dynamic system (solid line) in comparison with that from the direct spectral simulation (dashed line). Both are time averaged for 20 physical seconds.

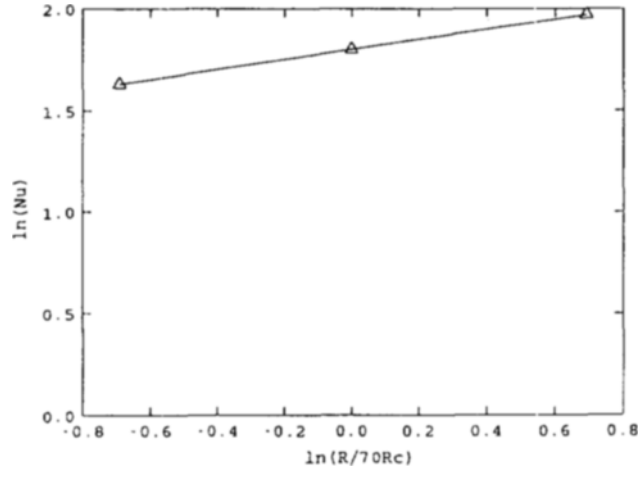

Fig. 9. Scaling of the Nusselt number versus the Rayleigh number for the range of $R=35R_C$ to $R=140R_C$. One hundred velocity eigenfunctions (MM=100) and one hundred temperature eigenfunctions (MT=100) are employed.

is displayed in Fig. 8 (time averaged for 20 seconds). The exact profile from the direct spectral simulation data is shown with dotted line in the same figure. The discrepancies are less than 5% in the Euclidean norm.

Next we would like to discuss how well a set of empirical eigenfunctions obtained at a reference Rayleigh number can be used at other Rayleigh numbers. In Fig. 9 are plotted time- and area-averaged Nusselt numbers at three different Rayleigh numbers, $R/R_c=35$, $R/R_c=70$ and $R/R_c=140$. These data are obtained by solving the low dimensional system (with 100 velocity and 100 temperature eigenfunctions) at the specific Rayleigh number for 20 physical seconds. Usually in the Rayleigh-Benard convection, the following scaling rule is valid.

$$Nu=\alpha\left(\frac{R}{R_C}\right)^n \tag{28}$$

where α and n are constants.

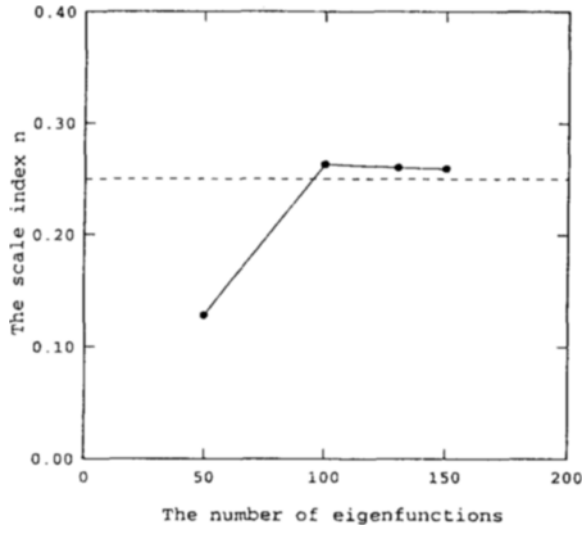

Fig. 10. The variation of the scaling index n with respect to the number of empirical eigenfunctions.

Table 1. Effects of number of eigenfunctions employed

	Nu at $R=70R_c$	n for $R=35R_c$-$140R_c$
Direct numerical simulation	5.75	0.250
150 eigenfunctions	5.91	0.259
130 eigenfunctions	5.97	0.260
100 eigenfunctions	6.05	0.263
50 eigenfunctions	6.15	0.128

The experimental or numerical value [Castaing et al., 1989; Garon and Goldstein, 1973] of n lies between 0.28 and 1/3. Here we obtained n=0.263, which is slightly smaller than the expected value. But a recent direct spectral simulation [Deane and Sirovich, 1991] using coarse meshes for $R<70R_c$ has yielded n=1/4. This difference in values of the index n is thought to be caused both by the free-shear boundary condition adopted in the present work and by the rather lower Rayleigh numbers, that are in contrast with the non-slip boundary condition and very high Rayleigh numbers used in Castaing [1989] and Garon [1973].

Now we change the number of eigenfunctions in the Galerkin procedure and investigate its effects on the performance of the resulting low dimension dynamic systems. If we use 50 velocity and 50 temperature eigenfunctions we get a much worse value n=0.128 even though the Nusselt number at the reference Rayleigh number ($70R_c$) is 6.15, which is not much different from the value obtained with 100 velocity and 100 temperature eigenfunctions, i.e., 6.05. This is because the set of reference empirical eigenfunctions, which was sufficient to resolve the boundary layer at the same Rayleigh number, is not fully appropriate (i.e., not optimal) for the resolution of the boundary layers at different Rayleigh numbers. The values of n for 130 velocity and 130 temperature eigenfunctions and for 150 velocity and 150 temperature eigenfunctions are 0.260 and 0.259, respectively. Fig. 10 plots the variation of n with respect to the number of empirical eigenfunctions and reveals that n has a tendency to approach 0.25 as the number of eigenfunctions increases. Therefore, we may conclude that a larger number of eigenfunctions is required to simulate flow field at Rayleigh numbers which are far different from the reference Rayleigh number. These findings are summarized in

Table 1.

Another cause of discrepancies between results of the low dimensional system and those of direct spectral simulation is the effects of neglected small scales that might be represented by the truncated empirical eigenfunctions with small eigenvalues. These small eddies act as eddy viscosity and eddy diffusivity in the dynamic of large eddies. The eddy viscosity and eddy diffusivity damp the dynamics of empirical eigenfunctions and consequently bring a decrease in Nusselt number. This explains why both the time-averaged Nusselt number from 100 velocity and 100 temperature eigenfunction system and that from 50 velocity and 50 temperature eigenfunctions are higher than the exact value from the pseudospectral simulation, the Nusselt number increases as the number of empirical eigenfunctions decreases. This is corroborated further by the results of 130 velocity and 130 temperature eigenfunctions and those of 150 velocity and 150 temperature eigenfunctions as shown in Table 1.

The observations of this section suggest that a wider range of parameter space can be simulated with the present low dimensional model obtained at a reference control parameter if the effect of small scale motion neglected due to the truncation in the Galerkin procedure and the changes in time averaged velocity and temperature profiles in the boundary layer are appropriately considered.

CONCLUSION

A low dimensional model which simulates the real fluid turbulence is derived. The phenomena which this model predicts include the time averaged flow patterns and heat transfer coefficient at the boundary (i.e. Nusselt number). Because this model is an optimal combination of empirical eigenfunctions of Karhunen-Loeve decomposition, in the sense that the maximum energy of turbulence is captured with a given number of degree of freedom, the dimension of this dynamic model is less than any other model when compared on the same criterion of accuracy. Due to this optimal property, even with a small number of degree of freedom the present model can take care of some important aspects of turbulent motions that determine heat and momentum transfer rates, which are usually affected by large scale energy containing motions. On the other hand the spatial intermittency and higher order derivative statistics may not be easily explained by the present low dimensional model. The maximum degree of freedom used in the present model is 300, which is far less than that used in the pseudospectral simulation of Boussinesq equation, i.e., 2×10^4. If some loss of accuracy in prediction can be tolerated, we may even reduce the number of equations to much smaller values.

It is also expected that the performance of the present low dimensional dynamic model can be improved further with appropriate considerations of small scale motions that are truncated in the Galerkin procedure and the variation of momentum and energy boundary layers as the value of the control parameter changes. This kind of investigation is currently under progress and shall be presented in a subsequent paper.

NOMENCLATURE

$a_n(t)$: spectral coefficient of the velocity field defined by Eq. (14)
$b_n(t)$: spectral coefficient of the temperature field defined by Eq. (15)
H : height of the system
$\mathbf{K}(\mathbf{x}, \mathbf{x}')$: two point correlation function defined by Eq. (10)
MM : number of velocity eigenfunctions employed
MT : number of temperature eigenfunctions employed
N : total number of snapshots used in the Karhunen-Loeve decomposition
Nu : Nusselt number (≡actual heat transfer/pure conduction heat transfer)
p : pressure
Pr : Prandtl number (≡heat capacity × viscosity/thermal conductivity)
R : Rayleigh number (≡gravity constant × thermal expansion coefficient × $(T_0-T_1)\times H^3$/thermal diffusivity × kinematic viscosity)
Re : Reynolds number (≡length × velocity × density/viscosity)
t : time
T : the deviation temperature
T_{total} : the system temperature
T_0 : the bottom temperature
T_1 : the top temperature
$\mathbf{u}$: velocity vector
u : x-component of the velocity vector
v : y-component of the velocity vector
w : z-component of the velocity vector

Greek Letters

ϕ : velocity eigenfunction
ψ : temperature eigenfunction
λ : eigenvalue
Ω : flow domain
ω : vorticity

Subscript

c : critical number

REFERENCES

Aubry, N., Holmes, P., Lumley, J. L. and Stone, E., "The Dynamics of Coherent Structures in the Wall Region of Turbulent Boundary Layers", *J. Fluid Mech.*, **192**, 115 (1988).

Brown, G. L. and Roshko, A., "On Density Effects and Large Structure in Turbulent Mixing Layers", *J. Fluid Mech.*, **64**, 775 (1974).

Canuto, C., Hussaini, M. Y., Quateroni, A. and Zang, T., "Spectral Methods in Fluid Dynamics", Springer-Verlag (1988).

Castaing, B., Gunaratne, G., Heslot, F., Kadanoff, L., Libchaber, A., Thomas, S., Wu, X. Z., Zaleske, S. and Zanetti, G., "Scaling of Hard Thermal Turbulence in Rayleigh-Bénard Convection", *J. Fluid Mech.*, **204**, 1 (1989).

Chandrasekhar, S., "Hydrodynamic and Hydromagnetic Stability", Oxford, Clarendon Press (1961).

Constantine, P., Foias, C., Manley, O. P. and Temam, R., "Determining Modes and Fractal Dimension of Turbulent Flows", *J. Fluid Mech.*, **150**, 427 (1985).

Deane, A. E. and Sirovich, L., "A Computational Study of Rayleigh-Benard Convection", *J. Fluid Mech.*, **222**, 231 (1991).

Garon, A. M. and Goldstein, R. J., "Velocity and Heat Transfer Measurements in Thermal Convection", *Phys. Fluids*, **16**, 1818 (1973).

Grötzbach, G., "Spatial Resolution Requirements for Direct Nu-

merical Simulation of the Rayleigh-Bénard Convection", *J. Comput. Phys.*, **491**, 241 (1983).

Herring, J. H. and Wyngaard, J., "Direct Numerical Simulation of Turbulent Rayleigh-Bénard Convection", in Fifth Symposium on Turbulent Shear Flows, 39, Springer, Berlin (1986).

Kessler, R., "Nonlinear Transition in Three-dimensional Convection", *J. Fluid Mech.*, **174**, 357 (1987).

Lumley, J. L., "The Structure of Inhomogeneous Turbulent Flows, in Atmospheric Turbulence and Radio Wave Propagation", ed. Yaglom, A. M. and Tatarski, V. I., pp. 166-176, Nauka, Moscow (1967).

McLaughlin, J. B. and Orszag, S. A., "Transition from Periodic to Chaotic Thermal Convection", *J. Fluid Mech.*, **122**, 123 (1982).

Park, H. and Sirovich, L., "Turbulent Thermal Convection in a Finite Domain: Numerical Results", *Phys. Fluids A*, **2**, 1659 (1990).

Silveston, P. L., "Wärmedurchgang in Waagerechten Flüssigkeitsschichten", *Forsch. Ing. Wes.*, **24**, 29 (1958).

Sirovich, L., "Turbulence and the Dynamics of Coherent Structures, Part I: Coherent Structures", *Quar. Appl. Math.*, Vol. XLV, **3**, 561 (1987a).

Sirovich, L. and Park, H., "Turbulent Thermal Convection in a Finite Domain: Theory", *Phys. Fluids A*, **2**, 1649 (1990).

Sirovich, L. and Rodriguez, J. D., "Coherent Structures and Chaos: A Model Problem", *Physics Letter A*, **190**(5), 211 (1987).

Sirovich, L., "Part III: Dynamics and Scaling", *Quar. Appl. Math.*, Vol. XLV, 583 (1987b).